Energy Spectra of Flow Past a Circular Cylinder

By SATYA PRAKASH SINGH AND SANJAY MITTAL

Department of Aerospace Engineering, Indian Institute of Technology, Kanpur, UP 208 016,
INDIA

Unsteady flow past a circular cylinder is computed for $100 \leqslant Re \leqslant 10^7$. A stabilized finite element formulation is utilized to solve the incompressible flow equations in the primitive variables form. Close to the cylinder and in the wake region, the finite element mesh has very high resolution. The phenomenon of *drag crisis* (sudden drop in drag v/s Re at $Re \sim 2 \times 10^5$) is captured by the present, two-dimensional, computations. With an increase in Re the transition point of the shear layer, separated from the cylinder surface, moves upstream. Our computations indicate that at the critical Re the instability reaches the point of flow separation and energizes the local flow causing it to re-attach. Energy spectra for these highly resolved flows at various Re are computed and the effect of various parameters involved in their calculation is investigated. It is found that despite the high shear in the flow, the kinetic energy shows the same structure as observed for 2D isotropic turbulence. For large Re flows it is found that the energy, $E(k)$, varies as $k^{-5/3}$ below the energy injection wave number and as k^{-3} for higher wave numbers.

---

1. Introduction

The flow past a circular cylinder undergoes several interesting changes as the Reynolds number is varied (Williamson (1996)). For low Reynolds numbers ($10 < Re < 47$) the flow separates from the cylinder surface and a pair of attached vortices appear in the wake. The flow is steady and symmetric about an axis passing through the center of the cylinder and along the free-stream direction. The vortices become stronger and larger with increase in Re. This arrangement becomes unstable beyond a certain critical Reynolds numbers ($Re \sim 47$) and von Karman vortex shedding takes place. At this point the flow is still two-dimensional and laminar. At $Re \sim 194$ the flow starts becoming three-dimensional due to the appearance of span-wise deformation of the vortices. Various modes of instabilities are observed as the Reynolds number is increased further. This marks the beginning of the transition of flow from laminar to turbulent. However, the boundary layer remains laminar. For Re larger than ~ 1000 the shear layer separating from the cylinder surface becomes unstable. The Kelvin-Helmholtz instability of the shear layer is believed to be a two-dimensional phenomenon (Braza, Chassaing & Ha Minh (1990)). With increase in Re the turbulent transition point for the separated shear layer moves upstream. At $Re \sim 2 \times 10^5$ the transition of the boundary layer flow to a turbulent state is observed. This is associated with a sudden decrease in the drag coefficient often referred to as *drag crisis*. Thereafter, for larger Re, the boundary layer achieves a fully developed turbulent state.

In the present work the two-dimensional flow past a cylinder is computed using a

stabilized finite element method. The mesh consists of a structured component occupying an annular ring close to the cylinder and an unstructured part, obtained via Delaunay triangulation, farther away from it. The mesh resolution is kept fine enough to capture the boundary layer and the related instabilities at all the Re considered. It is well known that the flow past a cylinder is three-dimensional beyond $Re \sim 200$. However, it is also believed that the Kelvin-Helmholtz instability of the separated shear layer is essentially two-dimensional. The present work is part of our effort to simulate the shear layer instability and study the mechanism of the transition of boundary layer to a turbulent state. The specific objective of this paper to study the energy spectrum for the flow past a cylinder at various Re ($100 \leqslant Re \leqslant 1 \times 10^7$). The results are compared to that for two-dimensional homogeneous isotropic turbulence. The effect of various parameters used in computing the energy spectrum from the finite element solution on an unstructured mesh is studied and presented.

In three-dimensional turbulence, energy injected into a flow system at a low wave number *cascades* to higher wave numbers via vortex stretching. In this *inertial range* the structure of energy density $E(k)$ is determined solely by the non-linear interactions while the total energy $\int E(k)dk$ is conserved. In the inertial range $E(k)$ varies as $k^{-5/3}$ down to the length scales where viscous effects cause a rapid decay of $E(k)$. In two-dimensional flows, the vortex stretching mechanism is absent. Consequently, both, energy ($\int E(k)dk$) and enstrophy (square of L^2 norm of vorticity, $\int_\Omega |\omega|^2 d\Omega$) are conserved. This implies that any flow of energy from low to high wave numbers is accompanied with another flux, back from small to larger length scales. This characteristic of two-dimensional turbulence is called *inverse cascade* (Kraichnan (1967)). The enstrophy cascade follows the k^{-3} law. More details on the structure of 2D turbulence can be found in Paret & Tabeling (1998), Frisch (1995), Kraichnan (1967), Doering & Gibbon (1995), Lesieur (1990).

There have been some efforts in computing flow past a cylinder at moderate to high Reynolds numbers. Selvam (1997) has carried out two-dimensional Large Eddy Simulation (LES). He observes the drag crisis but not to the same extent as indicated by the measurements. Furthermore, his results are sensitive to whether or not the Van Driest damping is utilized. The grids used are fairly coarse and the wake structure observed for high Re flows are very similar to that for laminar flows at much lower Re. Tamura, Ohta & Kuwahara (1990) have carried out computations without any turbulence model using a third order upwind finite difference scheme in two and three dimensions. For a certain choice of grid, they observe drag crisis. However, on increasing the number of grid points, the drag coefficient at $Re = 10^6$ increases significantly. Large Eddy Simulation (LES) of flow past a cylinder have been carried out by Kravchenko & Moin (2000) with a high order accurate scheme. The Reynolds number for their simulation is 3900. Good match with the experimental data was achieved. Simulations were also performed with and without the subgrid scale model. It was found that the mean velocity profiles from the two cases do not show any significant differences. However, the one-dimensional spectrum of velocity at a downstream location, shows a slower decay of energy at large wave numbers for the simulations without a subgrid scale model. Mittal & Moin (1997) have shown that for higher order upwind-biased finite difference schemes, the numerical viscosity removes substantial energy from the high wave number regime. They found that a central difference scheme does not suffer from such a problem but poses additional difficulties related to high dispersion errors. It was shown by Akin, Tezduyar, Ungor & Mittal (2002) that the numerical viscosity generated by the stabilization terms for the finite element formulation, being used here, are much larger than the eddy viscosity obtained using a Smagorinsky turbulence model except in regions very close to the

cylinder. In the present work, the finite element simulations are carried out on very fine grids without using any turbulence model.

The governing equations for the fluid flow are the incompressible Navier-Stokes equations. They are solved via a stabilized finite element formulation in the primitive variables. Equal-in-order linear basis functions for velocity and pressure are used and a 3 point Gaussian quadrature is employed for numerical integration. The non-linear equation systems resulting from the finite element discretization of the flow equations are solved using he Generalized Minimal RESidual (GMRES) technique(Saad & Schultz (1986)) in conjunction with diagonal preconditioners. The solution obtained from solving the Navier-Stokes equations over an unstructured mesh are interpolated on a structured mesh. The two-dimensional, discrete Fast Fourier Transform (FFT) of the velocity field is carried out by using the subroutines in the library from the Numerical Algorithm Group (NAG).

2. The governing equations

The spatial and temporal domains are denoted as $\overline{\Omega} \subset I\!\!R^2$ and $(0, T)$, respectively. $\mathbf{x}$ and t are the spatial and temporal coordinates and Γ represents the boundary of $\overline{\Omega}$. The Navier-Stokes equations governing incompressible fluid flow are

$$\rho(\frac{\partial \mathbf{u}}{\partial t} + \mathbf{u} \cdot \boldsymbol{\nabla}\mathbf{u} - \mathbf{f}) - \boldsymbol{\nabla} \cdot \boldsymbol{\sigma} = 0 \quad \text{on } \overline{\Omega} \ for \ (0, T), \tag{2.1}$$

$$\boldsymbol{\nabla} \cdot \mathbf{u} = 0 \quad \text{on } \overline{\Omega} \ for \ (0, T). \tag{2.2}$$

Here ρ, $\mathbf{u}$, $\mathbf{f}$ and $\boldsymbol{\sigma}$ are the density, velocity, body force and the stress tensor, respectively. The stress tensor is related to the velocity $\mathbf{u}$ and pressure p by $\boldsymbol{\sigma} = -p\mathbf{I} + \mathbf{T}$ where $\mathbf{T} = 2\mu\boldsymbol{\varepsilon}(\mathbf{u})$. Here $\mathbf{I}$ is the identity tensor, μ is the dynamic viscosity and $\boldsymbol{\varepsilon}(\mathbf{u}) = \frac{1}{2}((\boldsymbol{\nabla}\mathbf{u}) + (\boldsymbol{\nabla}\mathbf{u})^T)$. The boundary conditions are represented as $\mathbf{u} = \mathbf{g}$ on Γ_g and $\mathsf{n} \cdot \boldsymbol{\sigma} = \mathbf{h}$ on Γ_h where Γ_g and Γ_h are complementary subsets of the boundary Γ. The initial condition on the velocity is specified on $\overline{\Omega}$ as $\mathbf{u}(\mathbf{x}, 0) = \mathbf{u}_0$ on $\overline{\Omega}$, where $\mathbf{u}_0$ is divergence free.

3. The Fast Fourier Transform (FFT)

The velocity field obtained from the finite element formulation on the unstructured mesh is utilized to compute the energy spectrum. A structured mesh with $n \times m$ points, equally spaced in each direction, is created in a rectangular domain, Ω, of size $L_x \times L_y$. The velocity field $\mathbf{u}(x, y, t)$ is interpolated on this structured mesh. Its discrete Fourier transform is defined as (Press, Teukolsky, Vetterling, & Flannery (1992)):

$$\hat{\mathbf{u}}(k_x, k_y, t) = \frac{1}{\sqrt{mn}} \sum_{j_1=0}^{m-1} \sum_{j_2=0}^{n-1} \mathbf{u}(x, y, t) e^{-i(\frac{j_1 k_x}{m} + \frac{j_2 k_y}{n})}, \tag{3.1}$$

where, $k_x(n_1) = \frac{2\pi n_1}{L_x}$ and $k_y(n_2) = \frac{2\pi n_2}{L_y}$ are the wave numbers along the x and y directions, respectively. The index n_1 varies from $-n/2$ to $n/2$ while n_2 varies from $-m/2$ to $m/2$.
The inverse transform corresponding to equation 3.1 is given as

$$\mathbf{u}(x, y, t) = \sum_{k_x=0}^{m-1} \sum_{k_y=0}^{n-1} \hat{\mathbf{u}}(k_x, k_y, t) e^{i(\frac{j_1 k_x}{m} + \frac{j_2 k_y}{n})}. \tag{3.2}$$

The Fourier coefficients $\hat{\mathbf{u}}$ are the complex amplitudes of the modes labeled by the wave number k, where, $k = \sqrt{k_x^2 + k_y^2}$. The kinetic energy density in wave number space $\bar{E}(k)$ is defined as $\frac{1}{2}|\hat{\mathbf{u}}(k,\mathrm{t})|^2$. It is integrated over a thin shell of thickness $2\Delta k$ around k to give the contribution to the kinetic energy in the flow field from motion on the length scale $2\pi/k$. In the situation involving discrete wave numbers $E(k)$ can be represented as

$$E(k) = \sum_{k-\Delta k \leqslant k \leqslant k+\Delta k} \bar{E}(k_x, k_y). \tag{3.3}$$

N_k, the number of bands, each of thickness $2\Delta k$, are used to derive the energy spectrum from the FFT data. The various parameters that are needed to compute the energy spectrum, for a given velocity data on a certain finite element mesh, are the domain size $(L_x \times L_y)$, size of the structured mesh $(n \times m)$ and the number of wave number bands (N_k). The energy injection scale, for flow past a cylinder, is of the order of its diameter $(=2$ units in our case). The corresponding wave number, $k/2\pi$, is $1/2$.

4. Results

Details on the finite-element formulation can be found in papers by Tezduyar, Mittal, Ray & Shih (1992) and Mittal (2000). The formulation has been utilized, in the past, to solve unsteady flow past a circular cylinder at lower Re. (for example, see Mittal, Kumar & Raghuvanshi (1997)). Equal-in-order linear basis functions for velocity and pressure are used and a 3 point Gaussian quadrature is employed for numerical integration. The non-linear equation systems resulting from the finite element discretization of the flow equations are solved using the Generalized Minimal RESidual (GMRES) technique in conjunction with diagonal preconditioners.

4.1. *Boundary conditions*

The cylinder of diameter D resides in a rectangular computational domain whose upstream and downstream boundaries are located at $8D$ and $30D$ from the center of the cylinder, respectively. The upper and lower boundaries are placed at $8D$, each, from the cylinder. A schematic of the domain is shown in Figure 1. The no-slip condition is specified for the velocity on the cylinder surface while free-stream values are assigned for the velocity at the upstream boundary. At the downstream boundary a Neumann type boundary condition for the velocity is specified that corresponds to zero viscous stress vector. On the upper and lower surface boundaries the component of velocity normal to the component of stress vector along these boundaries is prescribed zero value. The Reynolds number is based on the diameter of the cylinder, free-stream velocity and viscosity of the fluid.

4.2. *Finite element mesh*

The finite element mesh consists of two parts. A structured mesh close to the cylinder provides the desired resolution to capture the boundary layer flow. It consists of N_t points in the circumferential direction. The radial thickness of the first layer of elements on the cylinder surface is h_r^1. Farther away from the cylinder, to save on the computational resources, an unstructured mesh is generated via Delaunay's triangulation. Figure 2 shows a typical mesh and its close-up around the cylinder. The various meshes used for the computations are given in Table 1. Most of the computations in this article have been carried out with a mesh consisting of $47,011$ nodes and $93,574$ elements (mesh $M2$).
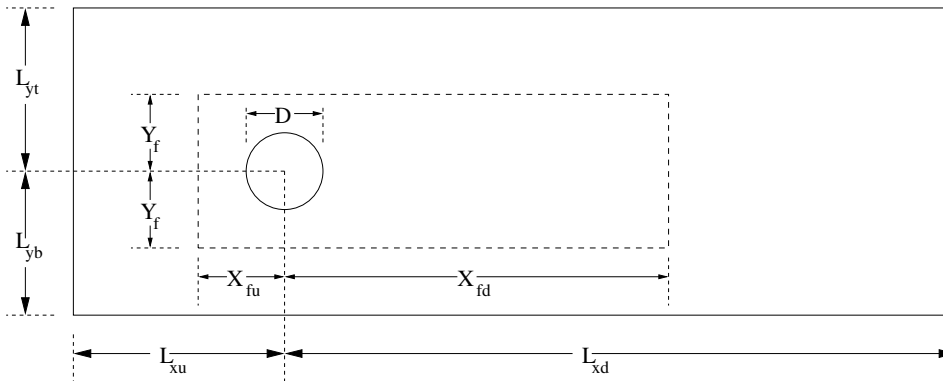
FIGURE 1. Flow past cylinder: schematic of the computational domain for the flow analysis (solid lines) and FFT (broken lines).

The time-averaged drag coefficient $(\overline{C}_D)$ from the computations for $Re = 10^6$ is 0.591. Computations on a much finer mesh with $116, 166$ nodes and $231, 484$ (mesh $M3$) result in a value of $\overline{C}_D = 0.607$. The time-averaged flows from the two meshes are also very close to each other. This suggests that mesh $M2$ is fine enough to capture most details that are significant in determining, at least, the mean flow. Later, it will be shown that the energy spectra from the two meshes are also almost identical.

Mesh	nodes	elements	h_r^1/D	N_t	Re
M1	34613	68858	5×10^{-3}	320	10^2
M2	47011	93574	5×10^{-5}	400	$10^4, 10^5, 10^6$
M3	116166	231484	5×10^{-6}	800	$10^6, 10^7$

Table 1. Flow past a cylinder at various Re: description of the finite element meshes employed.

4.3. *Overview of the solution at various Re*

Computations are carried out for $Re = 10^2$, 10^4, 10^5, 10^6 and 10^7. For each Reynolds number the time integration is continued till the unsteady solution is fully developed. This is monitored by observing the time histories of the aerodynamic coefficients and the velocity components at certain points in the wake of the cylinder. Figure 3 shows the instantaneous vorticity fields and their close-up views for the fully developed unsteady solution. The time averaged drag coefficient for $Re = 10^5$ is 1.07 while it is 0.607 and 0.897 for $Re = 10^6$ and 10^7, respectively. Clearly, the present computations are able to capture the phenomenon of *drag crisis*. The sudden drop in drag is accompanied with a narrowing of the wake. From Figure 3 it can be observed that the instability of the separated shear layer reaches the cylinder surface at $Re = 10^6$, thereby, energizing the boundary layer and causing it to re-attach.

4.4. *The Fast Fourier Transform (FFT)*

The solution obtained from the Navier-Stokes equations is interpolated on a structured mesh to compute the energy spectrum. The resolution of the mesh for the finite element computations is very fine close to the cylinder and it becomes coarser further away. For carrying out the FFT only a part of the original computational domain is utilized. It is
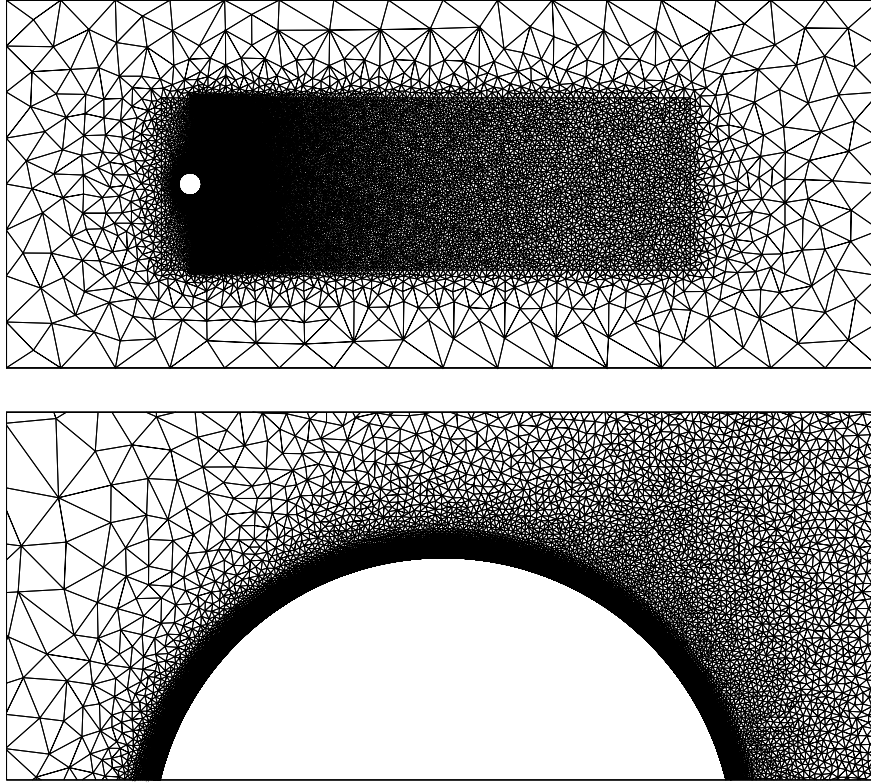
FIGURE 2. Flow past a cylinder: the finite element mesh $M2$ with $47,011$ nodes and $93,574$ triangular elements.

a rectangular region of size $L_x \times L_y$. The schematic of this choice of domain is shown in Figure 1. The number of grid points in the structured mesh is $n \times m$. Ideally, we would like to carry out the FFT on the entire finite element domain. We would also like the resolution of the structured mesh for FFT to match the finest resolution of the finite element mesh. However, this is is not possible because of the severe demands it places on computational resources. Therefore, for given computational resources, we can either compute with high resolution on a small domain or with moderate resolution on a large domain. While the grid spacing of the mesh restricts the maximum wave number that can be resolved, the size of the domain puts a limit on the lowest wave number that can be studied. The sensitivity of the various parameters on the energy spectrum is studied in the following subsections. The instantaneous solution for the fully developed unsteady flow for $Re = 10^6$ computed on mesh $M2$ is used to carry out these studies.

4.4.1. *Effect of periodicity of data*

Usually, the Fast Fourier Transform is useful for data sets that are periodic. The effect of lack of periodicity of data, in the present situation, is studied by comparing the results from the actual data set and a synthesized one. A new data set is constructed from the actual data by taking its mirror images about the x and y axes. The new data set is four times the size of the original one. The values of Y_f, X_{fu} and X_{fd} (indicated in Figure 1) for the domain considered for the study are $4D$, $4D$ and $15D$, respectively. It is observed that both the cases show very similar results and indicate the variation of $E(k)$ as k^{-3}.
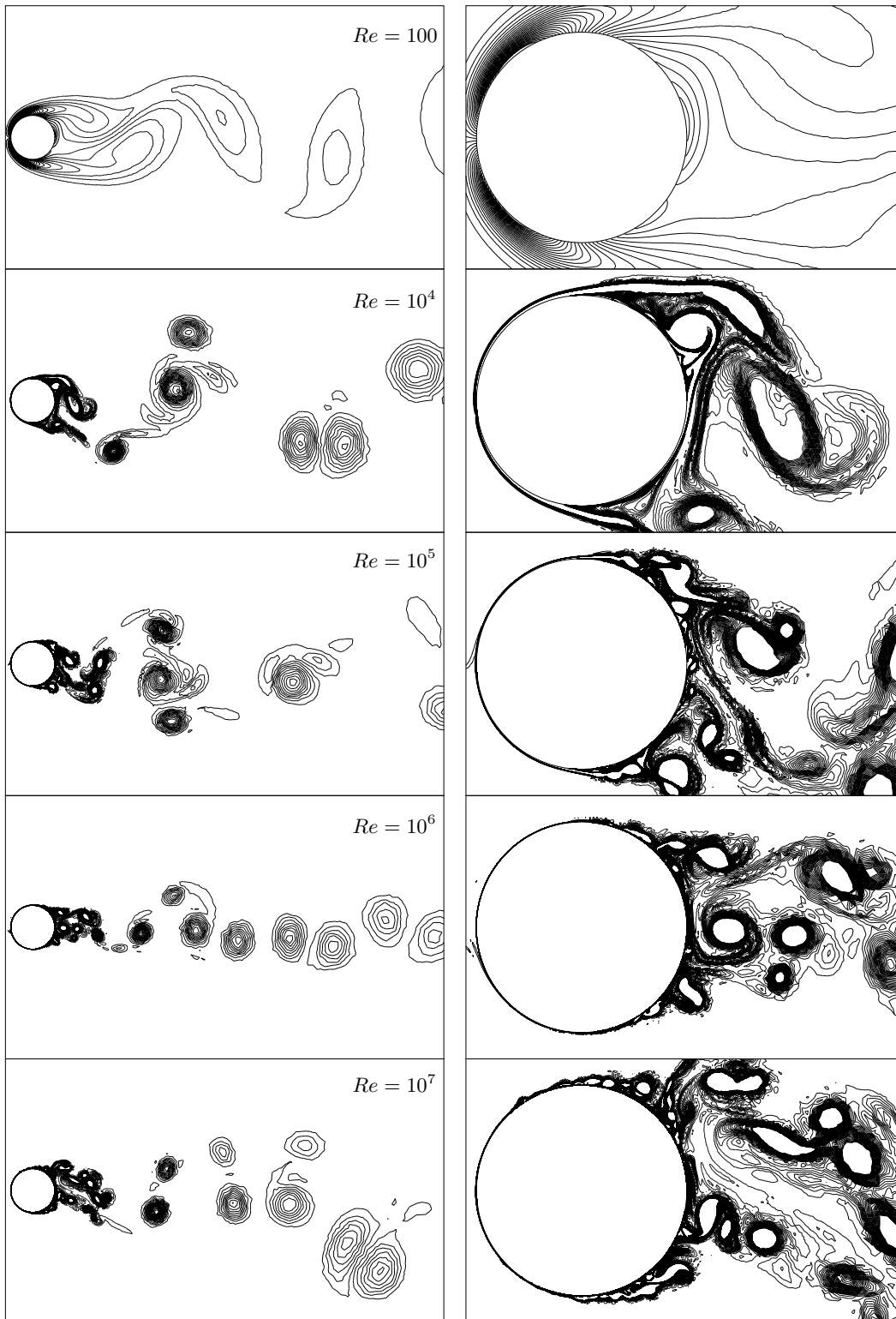
FIGURE 3. Flow past cylinder at various *Re*: instantaneous vorticity field and its close-up for the fully developed unsteady solution.

This study establishes that the lack of periodicity of the flow data is not a significant issue. In the remaining study, the actual (non-periodic) data set is employed.

4.4.2. *Effect of size of domain*

The finite element solution computed on mesh $M2$ is interpolated on four different structured meshes. Details of the various parameters used in this study are listed in Table 2. The grid size $(n \times m)$ for each case is chosen such that the resolution is same for all the four cases. Energy spectra for all the cases are shown in Figure 4. It is observed that the k^{-3} variation exists in all the cases whereas the $k^{-5/3}$ variation is seen only in the case with largest domain size $(L_x \times L_y = 38D \times 16D)$. The smaller length scale flow structures, corresponding to larger values of k, are mostly present in the vicinity of the cylinder and included in all the domains considered. Therefore, the k^{-3} variation is seen in all the cases. However, the large scale flow structures that correspond to smaller values of $k/2\pi$ are missed out in the domains of relatively small size. Therefore, the $k^{-5/3}$ variation of $E(k)$ is not observed for the smaller domains. This study shows that the size of the domain should be chosen depending on the range of wave numbers one wishes to resolve. Even though the location of the lateral boundaries beyond a certain distance, from the cylinder, may cease to affect the solution one may be forced to compute on a larger domain if energy spectrum is to be computed. It is also observed from Figure 4 that the domains $2.75D \times 2.75D$ and $2.75D \times 1.5D$ show very comparable results. This implies that the difference between the energy spectra using a square or rectangular domain is not significant.

Domain size $L_x \times L_y$	X_{fu}	X_{fd}	Y_f	grid size $n \times m$	N_k
$38D \times 16D$	$8D$	$30D$	$8D$	2432×1024	200
$19D \times 8D$	$4D$	$15D$	$4D$	1216×512	100
$2.75D \times 2.75D$	$1D$	$1.75D$	$1.375D$	176×176	100
$2.75D \times 1.5D$	$1D$	$1.75D$	$0.75D$	176×96	95

Table 2. Energy spectrum of flow past a cylinder at $Re = 10^6$: description of the various parameters for computing FFT on different domains.

4.4.3. *Effect of resolution*

Spacing between the nodes in the structured grid limits the largest wave number that can be resolved in the energy spectrum using FFT. As the number of nodes is increased, while keeping the domain size fixed, the resolution becomes better. The effect of resolution on the energy spectrum is studied for two domain sizes: $L_x \times L_y = 2.75D \times 1.5D$ and $38D \times 16D$. The results for the smaller and larger domains are shown in Figures 5 and 6, respectively. In both the cases the increase in grid points result in resolution of higher wave numbers. However, the basic structure of the variation of $E(k)$ remains same. As noted in the last section, the $k^{-5/3}$ variation of $E(k)$ is observed only for the large domain. It is also observed that, irrespective of the resolution of FFT, energy build-up occurs beyond a certain wave number. This implies that the piling up of energy at large wave numbers is not an artifact of the poor resolution for FFT but is intrinsic to the present finite element solution. This reflects the inadequacy of the present finite element mesh in resolving all the possible scales at such high Reynolds numbers. An appropriate turbulence model that will drain out the excess energy at large
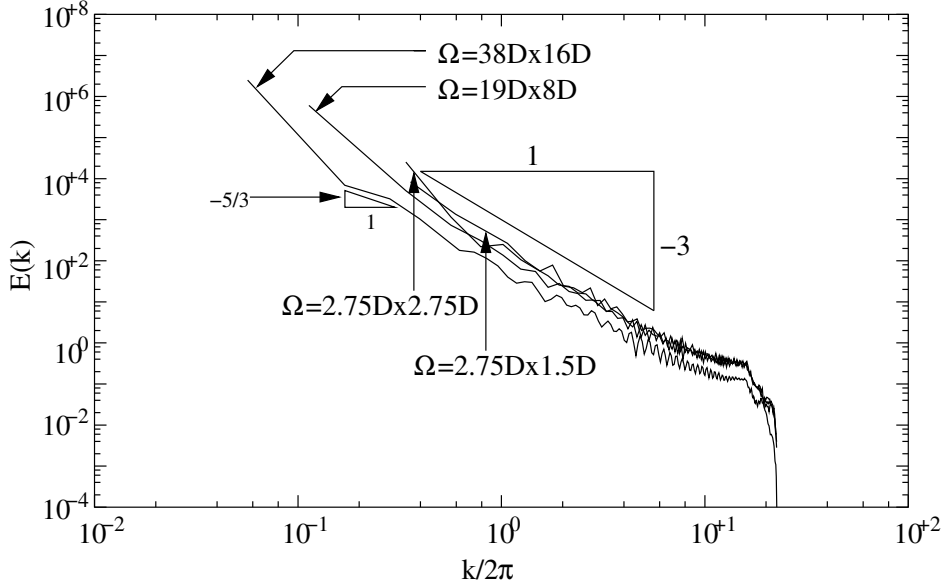
FIGURE 4. $Re = 10^6$ flow past cylinder: effect of domain size on the energy spectrum.

scales is needed (Mathieu & Scott (2000)). It was shown by Akin, Tezduyar, Ungor & Mittal (2002) that a Smagorinsky type of eddy viscosity model is not too effective for finite element computations using bilinear/linear interpolation functions. The eddy viscosity is overwhelmed by the numerical viscosity due to the stabilization terms. A similar conclusion was drawn by Mittal & Moin (1997) in the context of upwind-biased higher order finite difference schemes.

From Figure 6 we conclude that a grid with 1216×512 nodes is adequate for a domain of size $38D \times 16D$ to compute the energy spectrum.

4.4.4. *Effect of number of wave number bands (N_k)*

The energy spectrum $E(k)$ is obtained by integrating the energy density, $\bar{E}(k)$, over a thin band of thickness $2\Delta k$ around k. The entire wave number space is discretized into N_k equispaced bands of thickness $2\Delta k$. N_k is an important parameter in calculating the energy spectrum from the FFT data. If N_k is too large, then Δk is very small and not enough points are present in the band for computing a good average. However, if N_k is too small, the results are not expected to be accurate because the structure of $E(k)$ is lost in the averaging. Figure 7 shows the effect of N_k on energy spectrum. A smooth variation is observed for $N_k \sim 300$ while the spectrum becomes oscillatory at higher values of $k/2\pi$ when $N_k \sim 2000$. The k^{-3} variation of $E(k)$ is observed for all values of N_k. However, the $k^{-5/3}$ variation is a little sensitive to the choice of N_k. More work is needed to establish the nature of energy spectrum in this wave number regime. In the remaining study, unless it is mentioned otherwise, N_k is set to 300.

4.4.5. *Instantaneous v/s time-averaged spectrum*

Figure 8 shows the time-averaged spectrum for the unsteady data from, approximately, three periods of vortex shedding cycles. Also shown in the same figure is the spectrum obtained for an instantaneous velocity field. Both the results are very similar.
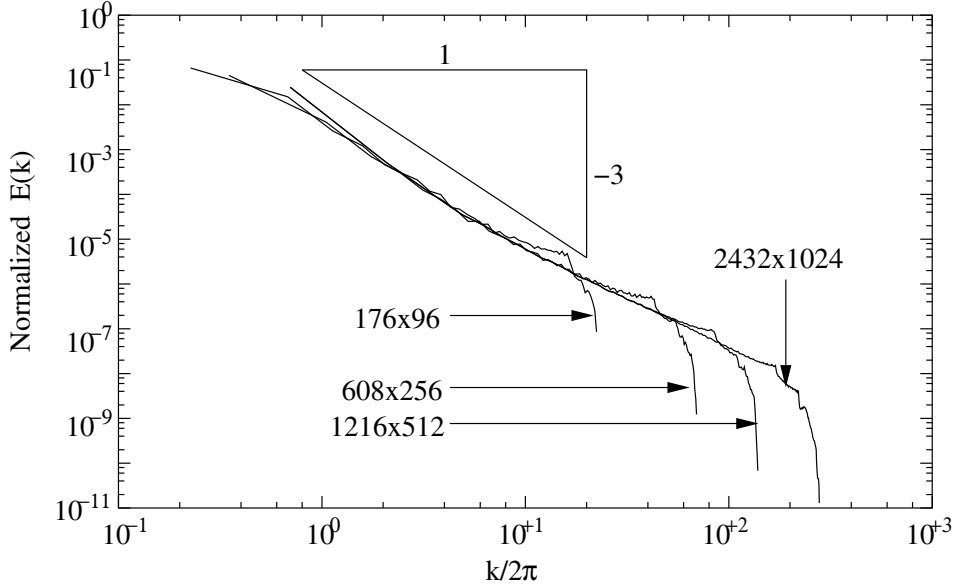
FIGURE 5. $Re = 10^6$ flow past cylinder: effect of the resolution of the FFT on the energy spectrum for the domain of size $2.75D \times 1.5D$.

4.4.6. *Effect of the resolution of the finite element mesh*

The time-averaged energy spectra are calculated for meshes $M2$ and $M3$ (see Table 1 for details on the meshes) are shown in Figure 9. The structured grid used for the FFT is same for both the finite element solutions. Both curves match each other in the moderate to high wave number region where $E(k)$ varies as k^{-3}. These results suggest that the mesh $M2$ is fine enough to study the energy spectrum of the flows at such high Reynolds numbers. However, the $k^{-5/3}$ variation is less prominent in the solution corresponding to mesh $M3$. At present, we are unable to explain this behavior and more work is needed to understand the energy cascade at lower wave numbers. Perhaps, the flow should be recomputed with a larger domain size so that more points are available in the low wave number regime.

4.4.7. *Effect of Reynolds number*

Figure 10 shows energy spectra for the flows at $Re = 100$, 10^4, 10^5, 10^6 and 10^7. The Re=10^5, 10^6 and 10^7 flows show very similar behavior and, both, the $k^{-5/3}$ and k^{-3} variations in $E(k)$ are observed. At $Re = 10^4$, the slope of the $E(k)$ v/s k curve is close to -3 for all k while, the $Re = 100$ flow does not show either of the two slopes. We conclude that the $Re = 100$ flow is laminar while it is turbulent for the other Re cases that have been studied. This is in line with the existing understanding of such flows. The wake starts becoming turbulent at $Re \sim 200$ but the transition of the boundary layer flow to turbulence begins at $Re \sim 2 \times 10^5$. It is quite remarkable that the turbulence for such highly sheared flows also displays the same structure as is observed for 2D isotropic, homogeneous turbulence. In all our computations the k^{-3} variation is consistently observed for high Re flows. However, the $k^{-5/3}$ variation of $E(k)$ is observed only for some cases.
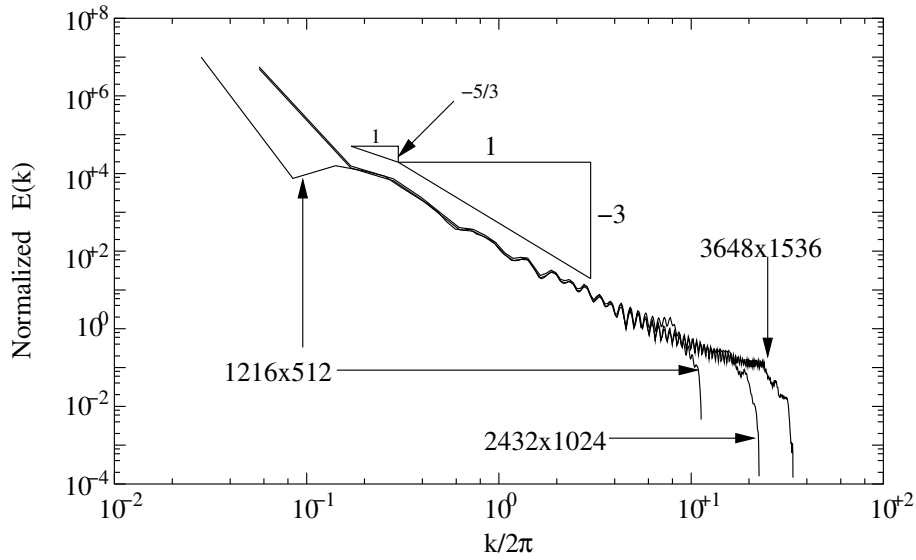
FIGURE 6. $Re = 10^6$ flow past cylinder: effect of the resolution of the FFT on the energy spectrum for the domain of size $38D \times 16D$.
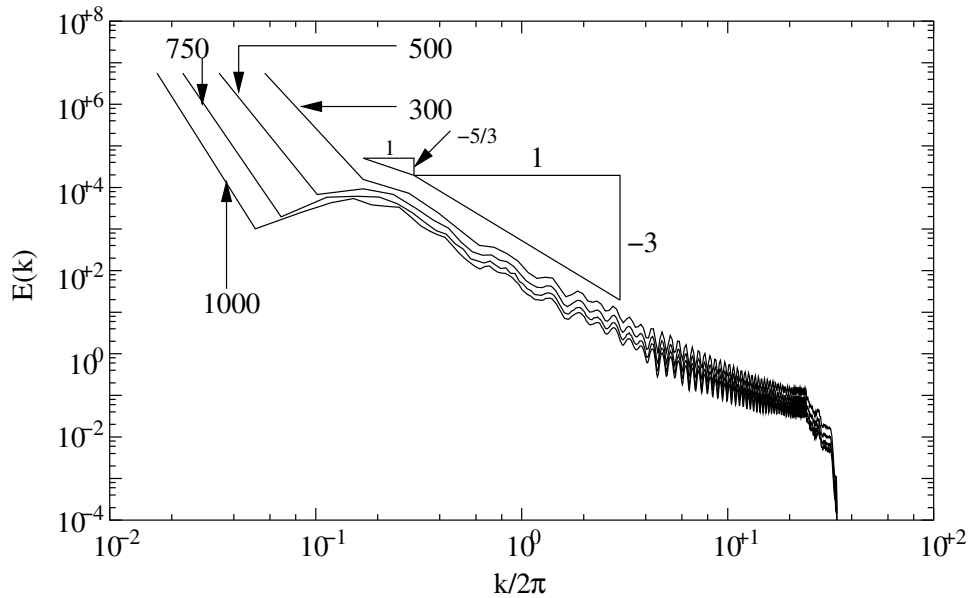

FIGURE 7. $Re = 10^6$ flow past cylinder: effect of number of wave number bands (N_k) on the energy spectrum.

4.4.8. *Power spectra of the time series*

Most of the features in the flow field that appear in the spatial description also appear in the temporal description of a field quantity reported at fixed point(s) in the flow. To further check the results that have been reported in this article, the power spectrum
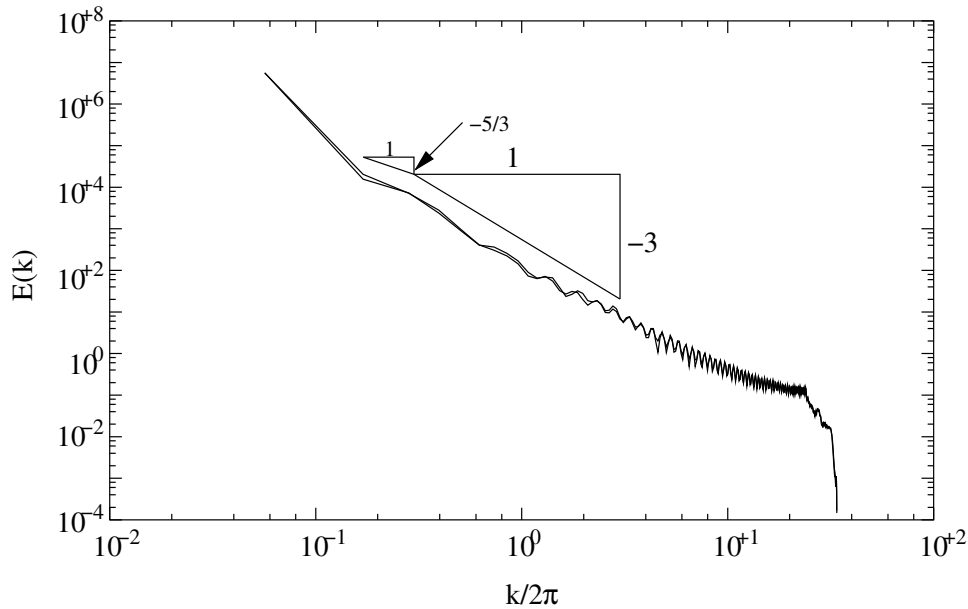
FIGURE 8. $Re = 10^6$ flow past cylinder: comparison of instantaneous and time-averaged energy spectrum.

corresponding to the time history of the velocity at a point in the wake has been studied. The result of this study for the $Re = 10^6$ flow, computed with the mesh $M3$, is shown in Figure 11. In this figure, the variation of the energy is shown with respect to the frequency which has been nondimensionalized with the cylinder diameter and free-stream speed. It can be observed that the power spectra obtained from, both, the temporal and spatial descriptions display the $k^{-5/3}$ and k^{-3} variation.

5. Conclusions

Results have been presented for computation of two-dimensional flow past a circular cylinder at Reynolds numbers ranging from 100 to 10^7. The sudden drop in the drag coefficient with increase in Re is predicted fairly accurately by the present computations. The Kelvin Helmholtz instability of the separated shear layer is captured very well in these simulations. The onset of the instability of the shear layer moves upstream as Re increases. At $Re = 10^6$ the shear layer becomes unstable right at the separation. This energizes the local flow and leads to its re-attachment. Consequently, the wake for the $Re = 10^6$ flow is much narrower than that for $Re = 10^5$.

The energy spectrum for flow at various Re has been studied. It is found that for $Re = 10^4$ and higher the energy spectrum resembles, very closely, the structure for 2D isotropic homogeneous turbulence. The k^{-3} variation of $E(k)$, beyond the energy injection wave number, is observed for all cases. In certain cases the $k^{-5/3}$ variation, below the energy injection wave number, is seen as well.

To establish confidence in these results the effect of various parameters on the energy spectrum was investigated. The flow field data was reflected about the cartesian axes to generate a periodic data set. No significant differences are noticed between the results for the actual and the synthesized periodic data. The effect of increasing the resolution of the
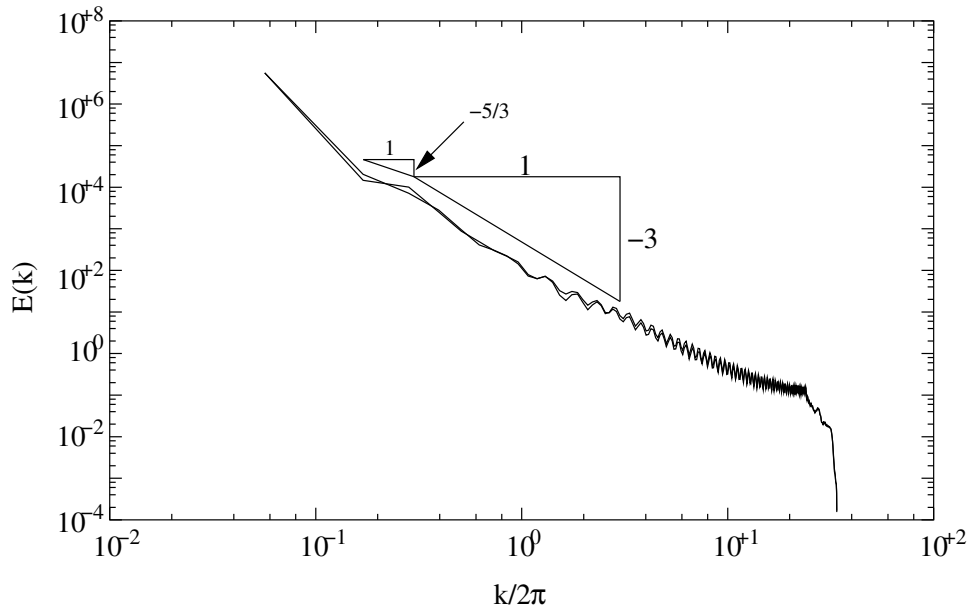
FIGURE 9. $Re = 10^6$ flow past cylinder: energy spectra for two different finite element meshes $M1$ and $M2$. The grid used for the FFT is same for both the finite element solutions.
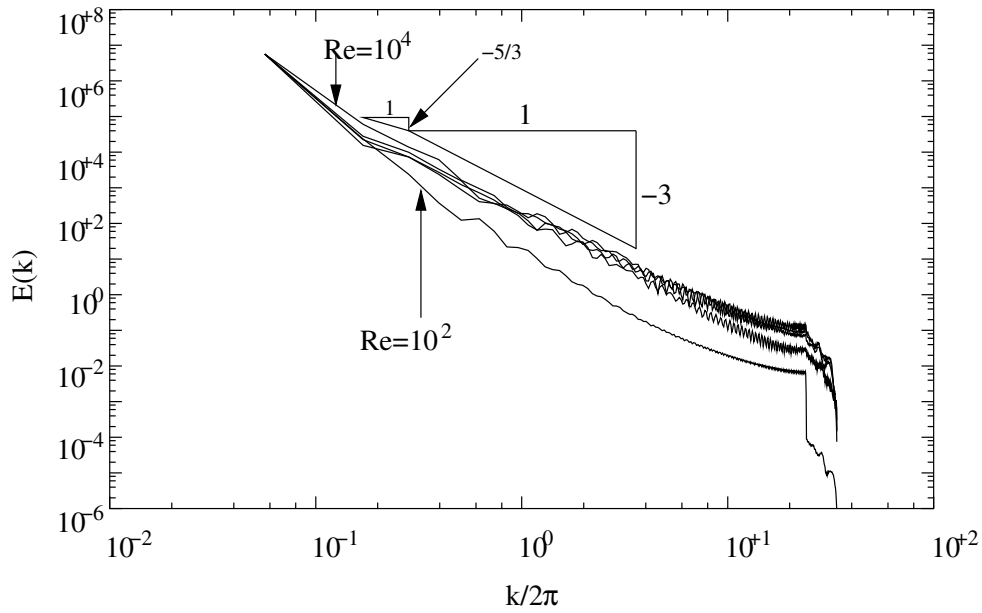

FIGURE 10. Flow past cylinder: energy spectra for various Re.

finite element mesh and the structured mesh for FFT was also studied. It is found that the base meshes, that have been utilized for solving the fluid flow and for FFT, provide sufficient resolution. The size of the domain limits the lowest wave number content in the simulations. It is observed that the $k^{-5/3}$ variation of $E(k)$ occurs only for the cases with large domain size. More work needs to be done, including computations with larger
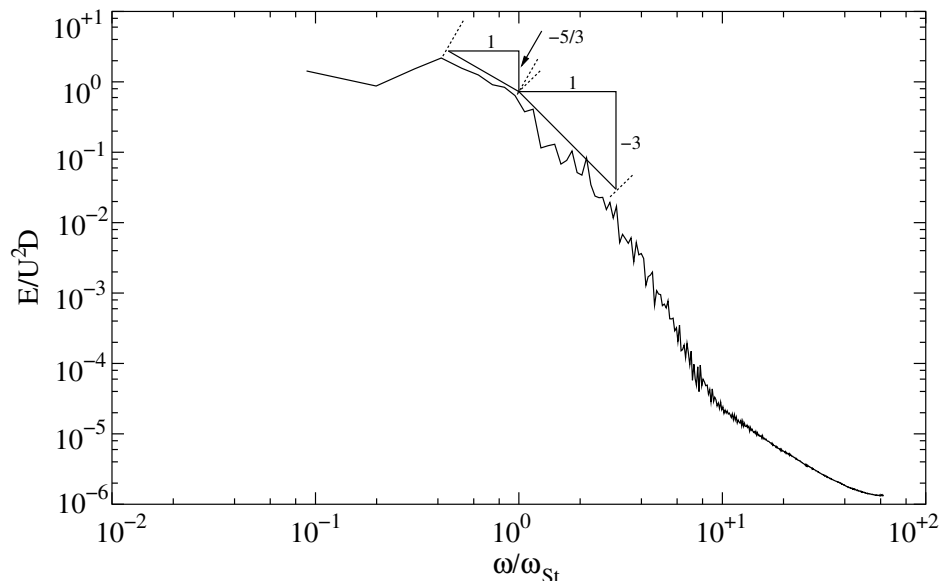
FIGURE 11. $Re = 10^6$ flow past cylinder: power spectra of the temporal variation of energy sampled at $(x/D = 0.26, y/D = -0.46)$.

domain size, to understand the $E(k)$ variation at low wave numbers. The high wave number content of the flow is mainly restricted to regions close to the cylinder. That is why, the k^{-3} variation of $E(k)$ is observed for all cases, irrespective of the size of domain.

REFERENCES

WILLIAMSON, C. H. K. (1996) Vortex dynamics in the cylinder wake. *Annual Review of Fluid Mechanics*, **28**, 477–539.

BRAZA, M., CHASSAING, P. & HA MINH, H. (1990) Prediction of large-scale transition features in the wake of a circular cylinder. *Physics of Fluids*, **2**, 1461.

KRAICHNAN R. H. 1967 Inertial ranges in two-dimensional turbulence. *Physics of Fluids* 1967 **10**, 1417–1423.

PARET, J. & TABELING, P. 1998 Intermittency in the two-dimensional inverse cascade of energy: Experimental observations. *Physics of Fluids* **10**, 3126–3136.

FRISCH, U. 1995 Turbulence. Cambridge University Press: Cambridge.

DOERING, C. R. & GIBBON, J. D. 1995 Applied analysis of the Navier-Stokes equations. Cambridge University Press: Cambridge.

LESIEUR, M. 1990 Turbulence in Fluids. Kluwer Academic Publishers.

SELVAM PANNEER R. (1997) Finite element modeling of flow around a circular cylinder using LES. *Journal of Wind Engineering and Industrial Aerodynamics*, **67 & 68**, 129–139.

TAMURA, T., OHTA, I. & KUWAHARA, K. (1990) On the reliability of two-dimensional simulation for unsteady flows around a cylinder-type structure. *Journal of Wind Engineering and Industrial Aerodynamics*, **35**, 275–298.

KRAVCHENKO A. G., & MOIN, P. (2000) Numerical simulation of flow over a circular cylinder at $Re_D = 3900$. *Physics of Fluids*, **12**, 403–413.

MITTAL, R. & MOIN, P. (1997) Suitability of Upwind-Biased-Finite Difference schemes for Large-Eddy Simulation of turbulent flows. *AIAA Journal*, **35**, 1415.

Akin, J.E., Tezduyar, T.E., Ungor, M. & Mittal, S. (2002) Stabilization Parameters and Smagorinsky Turbulence Model. to appear in *Journal of Applied Mechanics*,

Saad, Y. & Schultz, M. 1986 GMRES: A generalized minimal residual algorithm for solving nonsymmetric linear systems. *SIAM J. of Sc. and Stat. Comp.*, **7**, 856–869.

Press, W. H., Teukolsky, S. A., Vetterling, W. T. & Flannery, B. P. 1992 Numerical Recipes in FORTRAN. Cambridge University Press: Cambridge.

Tezduyar, T. E., Mittal, S., Ray, S. E. & Shih R. 1992 Incompressible flow computations with stabilized bilinear and linear equal-order-interpolation velocity-pressure elements. *Computer Meth. in App. Mech. and Engg.*, **95**, 221–242.

Mittal, S. (2000) On the performance of high aspect-ratio elements for incompressible flows. *Computer Meth. in App. Mech. and Engg.*, **188**, 269–287.

Mittal, S., Kumar, V. & Raghuvanshi, A. 1997 Unsteady incompressible flow past two cylinders in tandem and staggered arrangements. *Int. J. for Num. Meth. in Fluids* **25**, 1315–1344.

Mathieu, Jean & Scott, Julian 2000 An Introduction to Turbulent Flow. Cambridge University Press: Cambridge.